A41A-0007

TES Radiometric Assessment

E. Sarkissian, H. Worden, K. Bowman, B. Fisher, D. Rider, H. H. Aumann, M. Apolinski, R. C Debaca, S. Gluck, M. Madatyan, J. McDuffie
Jet Propulsion Laboratory, California Institute of Technology

D. Tremblay — Raytheon Information Solutions

M. Shephard, K. Cady-Pereira — Atmospheric and Environmental Research Inc. (AER)

D. Tobin, H. Revercomb — University of Wisconsin-Madison, Space Science and Engineering Center

ABSTRACT: TES is an infrared Fourier transform spectrometer on board the EOS-Aura spacecraft, launched 7/15/2004. Improvements to the radiometric calibration and consequent assessment of radiometric accuracy have been on-going since launch. The primary source of data used for radiance intercomparisons is AIRS on the Aqua platform, in the same orbit but about 15 minutes ahead of Aura. Scenes identified as homogenous to both AIRS and TES provide a basis set for testing improvements to the TES L1B calibration algorithm. Spectra from S-HIS on the WB-57 underflying Aura are also a valuable check on TES radiances because they provide spatial sampling on a smaller footprint than TES. We present the estimated radiometric accuracy of TES data currently available as well as the projected accuracy for future improvements based on prototyping results that include improvements to the L1B phase correction methods and model of temporal variability. We show agreement with AIRS to less than 0.5 K in observed brightness temperature using our latest calibration prototype.

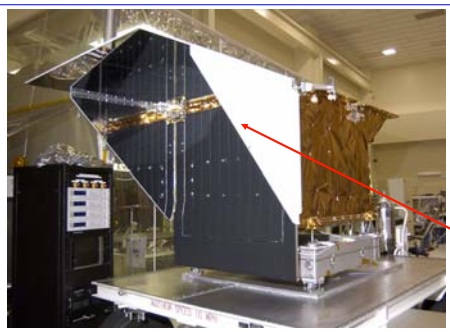

TES on EOS-Aura

TES OPTICAL SCHEMATIC

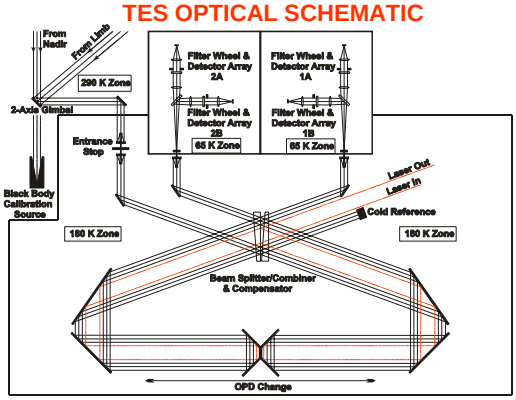

Table 1. TES Instrument Specifications

Spectrometer Type	Connes Type 4-port Fourier Transform Spectrometer
Max. Optical Path Difference	± 8.45 cm (nadir & calibration) ± 33.8 cm (limb); interchangeable
Scan (integration) Time	4 sec (nadir & calibration) 16 sec (limb)
Sampling Metrology	Nd:YAG laser
Spectral Resolution (unapodized)	0.06 cm^{-1} (nadir) 0.015 cm^{-1} (limb)
Spectral Coverage	650 to 3050 cm^{-1} (3.2 to 15.4 μm)
Detector Arrays	4 (1 x 16) arrays, optically-conjugated, all MCT PV @65 K
Field of Regard	45° cone about nadir; trailing limb or cold space; internal calibration sources
Pointing Accuracy	75 μrad pitch, 750 μrad yaw 1100 μrad roll
Max. Stare Time,	208 sec (40 nadir scans)
Spatial Resolution	0.5 x 5 km (nadir) 2.3 x 23 km (limb)
Radiometric Calibration	cavity blackbody (340K) + cold space view
Detector Array Co-alignment Calibration	Internal thin slit source

I. TES Level 1B Calibration Algorithm

Complex Calibration:

$$L_{sig} = \frac{C_{sig} - C_{CS}}{C_{BB} - C_{CS}} \varepsilon_{BB} B(T_{BB})$$

C_{CS} = cold space complex spectrum
C_{BB} = on-board blackbody complex spectrum
ε_{BB} = blackbody emissivity
$B(T_{BB})$ = Planck function for blackbody

$$C_{sig} = r(L_{sig} + L_{fo} - L_{cr} + L_{imr} e^{i\phi_1}) e^{i\phi} e^{2\pi mv/v_c}$$

$C = C(v, t)$ = complex spectrum
L_{sig} = target radiance
L_{fo} = foreoptics radiance
L_{cr} = cold reference radiance
L_{imr} = interferometer radiance
r = instrument response (radiometric slope)
ϕ_1 = phase of interferometer emission
ϕ = net optical and electronics phase
ϕ_1 = phase of interferometer emission
$2\pi mv/v_c$ = sampling phase (v_c = laser freq.)

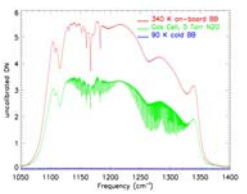

Sources of Error in Baseline L1B Calibration Algorithm
- Improper sampling phase alignment
- Model for time variability in response and offset
- Interferogram sampling jitter (phase modulation errors)

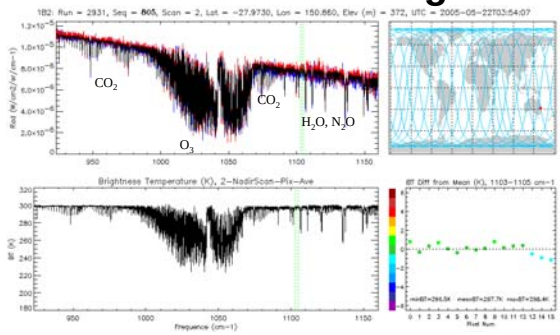

NADIR spectrum example for Australia, taken 5/22/2005. The detector average radiance with min/max (blue/red) are shown in the top right panel and average brightness temperature is shown in the bottom left panel. Right side panels show geolocation of the spectrum (top) and the variation of brightness temperatures across the detector array (bottom)

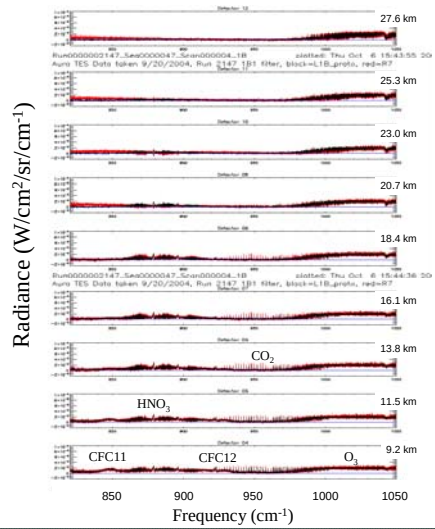

LIMB spectra for 63.1°N, 34.9° W, taken 9/20/2004. Spectra clearly show features due to Nitric Acid and CFC 11,12, with distinct altitude dependence. O_3, CO_2 and H_2O spectral lines are also visible. The surface is obscured by clouds (detectors viewing the surface are not shown). L1B calibration results corresponding to the baseline calibration (R7) are shown in red. Results from The latest L1B prototype algorithm are shown in black, with data processed at the spectral resolution normally used for the nadir view. Note improvements in the higher detectors where we expect a zero radiance level on the left part of the spectra.

Prototype for improved TES calibration

- Use of sampling phase information across detector arrays
  - -introduces inter-pixel dependency (code re-design)
  - -Improves limb and cold space alignment where phase is more indeterminate due to low signal levels.
- Adaptive frequency and pixel dependent cost function for sampling phase alignment.
- Model estimate for time dependent response and offset using calibration scans taken throughout global survey (16 orbits).
- Does not address interferogram sampling errors.
  - -Errors are only significant at edges of optical filters.
  - -Mitigated by spectral selection in L2.

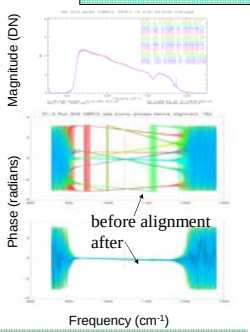

Example of sampling phase alignment

Estimation of instrument response and offset

The uncalibrated OBRCS (on-board radiometric calibration source or *BB* at temperature *T*) and cold space (*CS*) spectra can be related to the instrument response (R) and offset (S):

$$C_{BB}(v,t) = R(v,t)B(v,t,T) + S(v,t) + n$$
$$C_{CS}(v,t) = S(v,t) + n$$

With averages for N observations:

$$\bar{C}_{BB}(v) = \frac{1}{N}\sum_{i=1}^{N} C_{BB}(v,t_i)$$
$$\bar{S}(v) = \frac{1}{N}\sum_{i=1}^{N} C_{CS}(v,t_i)$$
$$\bar{R}(v) = \frac{\bar{C}_{BB}(v) - \bar{S}(v)}{B(v,T)}$$

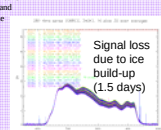

The instrument response and offset for a given pair of BB and CS observations (with measurement times t_i and t_j) is modeled as:

$$C_{BB}(v,t_i) = \alpha(v,t_i)\bar{R}(v)B(v,t_i,T) + \beta(v,t_i)\bar{S}(v) + n$$
$$C_{CS}(v,t_j) = \beta(v,t_j)\bar{S}(v) + n$$

Assuming $\beta(v,t_i) \approx \beta(v,t_j) \quad |t_i - t_j| < \varepsilon$

We modify the BB and CS calibration spectra by:

$$\begin{pmatrix} C_{BB} \\ C_{CS} \end{pmatrix} = \begin{pmatrix} \bar{R}(v)B(v,t_i,T) & \bar{S}(v) \\ 0 & \bar{S}(v) \end{pmatrix} \begin{pmatrix} \alpha \\ \beta \end{pmatrix}$$

http://tes.jpl.nasa.gov

II. AIRS-TES Radiance Comparisons

Applying AIRS SRF to TES spectra:
Test with simulated data

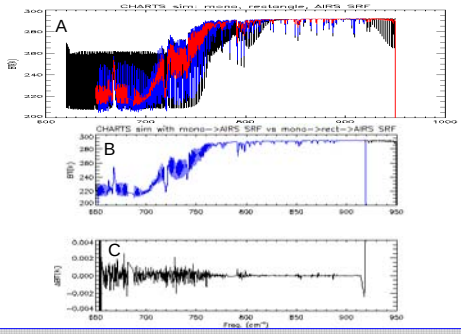

Top panel (A) shows a simulated, unconvolved (monochromatic) spectrum in black compared to spectra convolved with the TES instrument line shape (ILS), a simple sinc function, in blue and the AIRS spectral response function (SRF) in red. Panel (B) shows the monochromatic spectrum convolved directly with AIRS SRF (red) overplotted with the same spectrum convolved first with TES ILS followed by AIRS SRF (blue). Bottom panel (C) is the difference between a direct AIRS SRF convolution and the convolution with TES ILS followed by AIRS SRF. Difference in brightness temperature is well below theTES noise equivalent delta-temperature (NEDT) and confirms the radiance comparison method.

Brightness Temperature Comparison

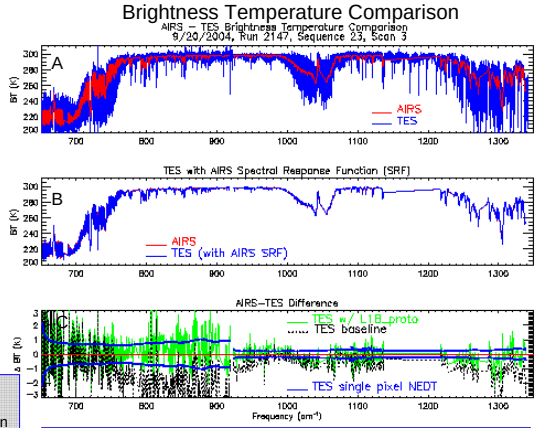

Top panel (A) shows a direct brightness temperature comparison for a selected, homogenous nadir target, TES pixel #8. Panel (B) shows that same comparison after the AIRS SRF is applied to the TES data. Panel (C) shows AIRS-TES differences compared to the TES NEDT: black dots show our baseline calibration results and green line shows the difference after using the L1B prototype with improved algorithms.

Ensemble comparisons vs. radiance and frequency:
Test of TES L1B algorithm improvement

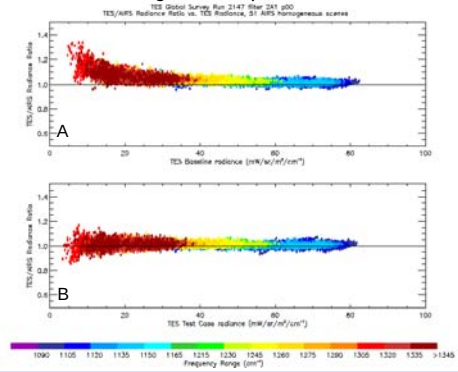

After identifying 190 TES nadir targets (from a 16-orbit Global Survey) with 0.5 K homogeneity across a detector array, 50 of these were confirmed as homogenous for AIRS also. These homogenous nadir targets are the test cases for TES L1B algorithm improvements. Both plots show the radiance ratio (TES/AIRS) vs. radiance and color coded for frequency ranges. Panel (A) shows the spread in values over the homogenous cases for the baseline calibration; panel (B) shows this for the prototype improved calibration (Test Case).

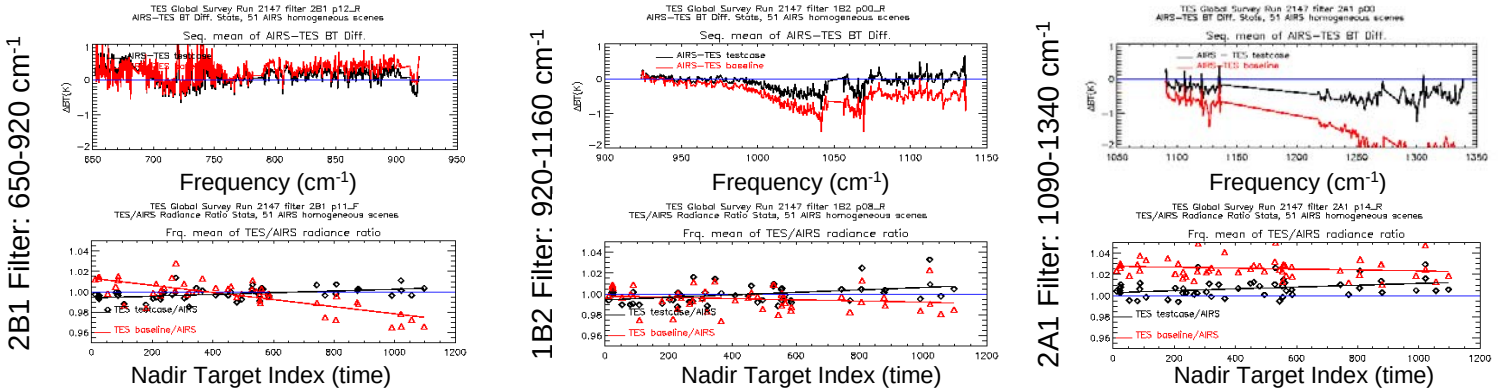

Frequency and time dependence of AIRS-TES comparisons for TES 2B1, 1B2 and 2A1 filters. For each filter, the top panel shows the average over 50 nadir targets of the AIRS-TES brightness temperature difference as a function of frequency on the AIRS frequency grid. (TES data are for a single pixel and have been convolved with the AIRS SRF). The bottom panels show averages over frequency as a function of target index or time - spanning about 26 hours. These plots demonstrate how the different prototype improvements affect our frequency ranges. In the 2B1 filter, the most significant improvement is from modeling the time dependence, while in 1B2 and 2A1, the time dependence is nearly flat in both the baseline and prototype runs, as expected from the spectral dependence of ice absorption. For 1B2, and especially 2A1, we see large improvements due primarily to the improved sampling phase alignment algorithm.

III. SHIS-TES Radiance Comparisons

10/31/04 AVE Flight

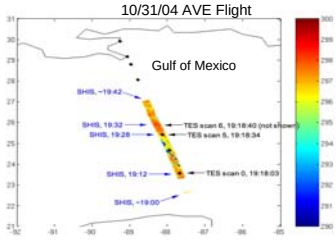

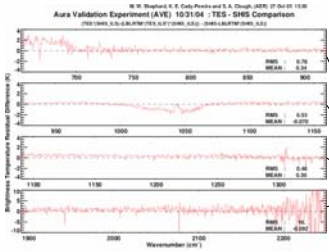

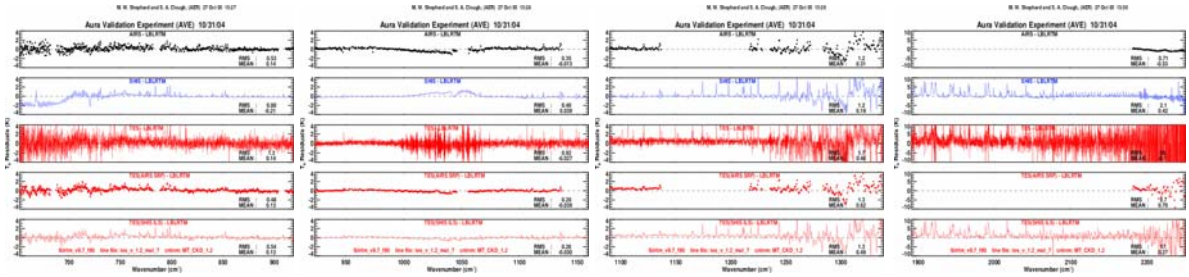

Comparisons of AIRS, SHIS and TES (with different spectral convolutions) to LBLRTM (Line-By-Line Radiative Transfer Model) using GMAO profiles as input. The four horizontal panels are for TES filters 2B1, 1B2, 2A1 and 1A1, respectively, with frequency ranges as noted.

Direct TES-SHIS comparisons over TES frequency ranges. Data from both instruments were reconvolved with the ILS of the other for the brightness temperature difference.

Next steps: Use of retrieved profiles in LBLRTM for both TES and SHIS

IV. Summary and Outlook

Table 2. AIRS-TES Comparison Summary

TES Filter	Freq. Range (cm^{-1})	Mean AIRS-TES Δ BT (K)		RMS AIRS-TES Δ BT (K)	
		Run 2147 9/20/2004	Run 2931 5/21/2005	Run 2147 9/20/2004	Run 2931 5/21/2005
2B1	650 - 920	0.18 (0.29)	0.13 (0.31)	0.46 (0.86)	0.42 (0.54)
1B2	920 - 1160	-0.01 (0.05)	0.12 (0.19)	0.48 (0.52)	0.38 (0.38)
2A1	1090 - 1340	-0.34 (-1.05)	-0.35 (-1.37)	0.36 (0.37)	0.32 (0.70)

Comparison results are shown for TES runs taken on two different days. The numbers are the mean and rms of brightness temperature differences (Δ BT in K) averaged over frequency, 16 TES detectors and nadir target scenes (50 targets for run 2147 and 320 for run 2931). Brightness temperature differences are given for the L1B prototype results with baseline L1B comparisons in parenthesis ().

Bias and RMS for AIRS-TES differences are < 0.5 K for improved TES L1B calibration

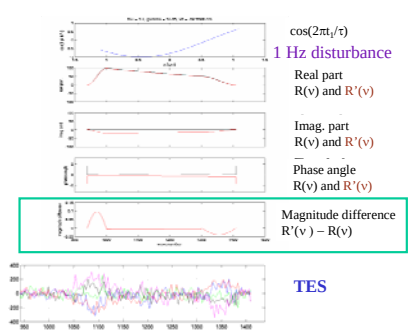

Model produced by H. Revercomb and D. Tobin, *et al.* (U. Wisc.) to simulate TES spectral errors due to interferogram sampling jitter.

CONCLUSIONS:

The improvements to the TES L1B algorithm will produce TES spectra with an accuracy sufficient for quantitative analyses using TES L2 retrievals.

Remaining errors in TES radiance spectra, such as those due to inter-ferogram sampling jitter (phase modulation) are under investigation for detection and possible correction methods. They are currently mitigated by selection of frequency ranges in the L2 retrieval that do no include filter band edges.